

Nano-structured calcium silicate hydrate-based composites derived from fluosilicic acid for highly efficient Cr(III) removal and methylene blue degradation from wastewater

Rui Ma, Jie Gao, Xinhua Zhu, Jun Li, Yubin Wang, Jianhong Luo*

Department of Chemical Engineering, Sichuan University, Chengdu, Sichuan 610065, China, emails: luojianhong@scu.edu.cn (J. Luo), maruiscu@163.com (R. Ma), gjscu2018@163.com (J. Gao), zhuxinhua19@163.com (X. Zhu), lijun@scu.edu.cn (J. Li), wyb9401@126.com (Y. Wang)

Received 15 August 2019; Accepted 3 February 2020

ABSTRACT

Herein, fluosilicic acid, a by-product generated from the wet process of phosphoric acid, is successfully used to synthesize silica substrate. Then three novel adsorbents calcium silicate hydrates (CSH), Al modified CSH (Al-CSH) and F modified CSH (F-CSH) are synthesized from this silica substrate and used as adsorbents to remove Cr(III). Consequently, the largest surface area and abundant pore structure render Al-CSH the best performance for Cr(III) removal. The combination of characterization (X-ray diffraction, Brunauer–Emmett–Teller, scanning electron microscopy, X-ray photoelectron spectroscopy, and UV–Vis) and kinetic experiments reveal the adsorption of Al-CSH proceeds through an ion-exchange mechanism, which follows pseudo-second-order kinetics and Langmuir adsorption model. Moreover, the obtained Cr-bearing Al-CSH could be converted into an efficient photocatalyst by annealing at 300°C/Air, which shows excellent degradation efficiency of 94% for methylene blue during five cycles. This work proposes a route “waste → adsorbent → catalyst”, which is significant for waste utilization and water purification.

Keywords: Modified calcium silicate hydrate; Chromium (III) adsorption; Reaction kinetics; Mechanism; Photocatalyst

1. Introduction

The extensive application of leather tanning, metallurgy and electroplating process has caused serious chromium contamination [1]. Cr features at non-biodegradable and will be accumulated in biological tissues, at the same time, various diseases and disorders will be caused by its teratogenic and carcinogenic properties [2,3], therefore removal of Cr(III) from wastewater is imperative [4]. At present, a couple of methods have been used to remove Cr(III) from wastewater including chemical precipitation [5], adsorption [6], ion exchange with synthetic resins [7], electrolysis [1], etc. Adsorption is generally regarded as the most effective

technology with advantages of low cost and easy handle processes [8,9].

In recent years, calcium silicate hydrates (CSH), a new kind of eco-friendly material [10] with a special crystal structure and high-efficiency adsorption capacity for heavy metal ions, is widely concerned. Shao et al [11] used the combined activator of sodium silicate and sodium hydroxide to synthesis the CSH to remove Cu^{2+} , the optimal adsorption capacity is greater than 100 mg/g. Baldermann et al [12] synthesized the CSH by a sol–gel process and explored the immobilization mechanism. Zhang et al [13] used the phosphate-rich product HAP/CSH as a composite adsorbent to remove Pb(II) from aqueous solution, the adsorption capacities of Pb(II) HAP/CSH could reach 946.7 mg/g.

* Corresponding author.

Lihua et al [14] used post-grafting with calcium nitrate tetrahydrate and sodium metasilicate nonahydrate to synthesize MCS-SH, which exhibited excellent performance as adsorption material for Cd^{2+} , Cu^{2+} , Pb^{2+} , and Cr^{3+} . However, most of the reported CSH are synthesized from Na_2SiO_3 [15,16] or tetraethyl orthosilicate [17]. Nevertheless, chemical reagent-derived CSH fails to meet the requirement of low cost, easy access, and convenient application for industry scale [18].

Herein, our research team proposes to prepare calcium silicate from fluosilicic acid, which is a by-product of wet-process phosphoric acid and has a huge output in China. Generally, at least 0.05t of fluosilicic acid (100% H_2SiF_6) by-product is produced for every one ton of wet-process phosphoric acid (100% P_2O_5) or procalcium (100% P_2O_5) produced in the phosphorus chemical industry [19]. In 2016, the world's output of phosphate fertilizer was 44.5 million tons, equivalent to about 2,235,000 tons of fluosilicic acid [20]. Most importantly, fluosilicic acid contains a large amount of silicon, which has considerable economic feasibility if it is used as a silicon source for CSH synthesis. At present, there are few studies on new ways of utilizing silicon source in fluosilicic acid. Hence, a novel method of synthesizing the CSH from fluosilicic acid is explored in this work. At the same time, the CSH has a crystal structure and the ionic radius similarity to that of hydroxyapatite, which means that the Ca^{2+} in the lattice can be exchanged by certain cations (Pb^{2+} , Cd^{2+} , Zn^{2+} , Hg^{2+} , etc.), and the SiO_3^{2-} in structure can be exchanged by certain anions such as F^- , HCO_3^- , etc. [21]. NaF and Al_2O_3 are also applied to modify the CSH to change its performance in the removal of Cr. However, CSH is usually easily soluble in low-pH aqueous solutions [18], which makes it infeasible to desorb the heavy metal ions bearing CSH for re-adsorption. To solve this problem, the Cr bearing CSH is transferred into photocatalyst by calcined for recycling.

This work consists of four aspects: (1) testing the effect of Cr concentration, adsorbent dose, temperature and pH on the removal efficiency, (2) exploring possible adsorption mechanisms via characterization [X-ray diffraction (XRD), X-ray photoelectron spectroscopy (XPS), scanning electron microscopy (SEM), EDS, Brunauer–Emmett–Teller (BET)] of Al-CSH, (3) performing adsorption isotherms, kinetics analysis, and thermodynamic studies and (4) recycle experiment about the Al-CSH adsorbent containing Cr as photocatalyst for methylene blue degradation. This work provides a novel strategy for waste utilization and water purification through the route of “waste \rightarrow adsorbent \rightarrow catalyst”, which shows great economic value.

2. Materials and methods

2.1. Materials

Fluosilicic acid (AR), ammonia water (AR) are purchased from Chengdu Jinshan Chemical Reagent Co., Ltd. (China). Calcium hydroxide (AR), chromic nitrate (AR), nitric acid (AR), Urea (AR) and alumina (AR) are purchased from Chengdu Kelong Chemical Co., Ltd. (China). Sodium fluoride (AR) is purchased from Chengdu Shudu Equipment Manufacturing Co., Ltd. (China). Deionized water is

produced by the Aquapro water making machine (ABZ1-1001-P, Aquapro, China) in the laboratory. Stock solutions of Cr(III) of 400 mg/L are prepared by dissolving a certain amount of chromic nitrate into deionized water.

2.2. Preparation of silica

The silica is synthesized from the mixture of fluosilicic acid and ammonia by a co-precipitation method, and the mole ratio of fluosilicic acid and ammonia is set as 1:6. Firstly, fluosilicic acid and ammonia are diluted with equal volume of deionized water, then the diluted fluosilicic acid is stirred at 150–200 r/min, aqueous ammonia is continuously added to the stirring fluosilicic acid solution at a speed of 0.3–0.4 ml/s. Then, the mixture is filtered and washed to pH = 7 with deionized water and dried at 105°C for 5 h in an oven.

2.3. Preparation of CSH and modified CSH

For the CSH, the molar ratio of calcium and silica is 0.7/1 [22]. The modified CSH is composed of silica/calcium hydroxide/dopant (sodium fluoride, alumina) as a molar ratio of 1/0.7/0.05. Then the subsequent synthesis process is similar to the hydrothermal method as reported in the literature [21] (CJ-0.5, Weihai Xinyuan Chemical Co., Ltd., China).

2.4. Material characterization

A pH meter (PHS-3C, INESA) is employed for measuring pH values of the aqueous phase. The chemical compositions are analyzed by an X-ray powder diffractometer (XRD) (CX-2700, Dandong HaoYuan Instrument Co., Ltd., China) with Cu $\text{K}\alpha$ radiation in a scanning range of 10°–90° (2 θ). The surface areas and total pore volumes of the three adsorbents are measured by using N_2 adsorption/desorption isotherms performed at 77 K with a BET specific surface tester (ASAP 2020 PLUS HD 88, Micromeritics, America) and the BET method. SEM images are recorded using an SEM (JSM-IT100, JEOL Ltd., Japan) for observing surface morphology and identifying the elements of the samples. X-ray photoelectron spectroscopy (XPS, XSAM 800, Kratos, England) Al-CSH before and after adsorption are also performed to investigate the possible adsorption mechanism, and all binding energies (BEs) are referenced to the C1s hydrocarbon peak at 284.8 eV.

2.5. Analysis

The residual concentration of Cr(III) is detected by the spectrophotometric method (GB7466-87) with an ultraviolet spectrophotometer (UV-1100, Shanghai shine Instrument Co., Ltd., China). The linear equation of the standard curve ($Y = 1.5834X - 0.0008$, the correlation coefficient of 0.9997) is obtained in the experiment to determine unknown concentrations. The metal ions contents in the heavy metal mixture are examined by using the inductively coupled plasma spectrometer (ICP-AES, ARCOS, Germany).

The capacity of adsorbent can be calculated by Eq. (1) and the removal efficiency is defined by Eq. (2):

$$q = \frac{(C_0 - C_t) \times V}{m} \quad (1)$$

$$x = \frac{C_0 - C_t}{C_0} \times 100\% \quad (2)$$

where q is the amount of Cr(III) adsorbed per unit mass of adsorbent (mg/g), C_t is the residual Cr(III) concentration of in the simulated solution (mg/L), C_0 is the initial Cr(III) concentration (mg/L), m is the mass of adsorbent (mg) and V is the volume of the simulated solution (L).

2.6. Reusability experiment

CSH features at easy soluble in low-pH aqueous solutions [18], which makes it difficult to regenerate. To solve this problem, a facile strategy to convert the Cr-bearing Al-CSH into an effective photocatalyst by a simple heating process is proposed in this work. By simple annealing treatment at 300°C/air for 2 h, Cr-bearing Al-CSH is successfully converted into an efficient photocatalyst for methylene blue (MB) degradation.

The photocatalytic activity of samples is evaluated via the photocatalytic degradation of MB. A 300 W simulated solar Xe lamp (NAI-GHY-DSGGH, Shanghai Nai Precision Instrument Co., Ltd., China) is employed as the visible light irradiation source. The photocatalytic degradation of MB is conducted in a 30 ml quartz tube, the distance between the light and MB solution surface is kept at 5 cm, and the reaction temperature is kept at room temperature. The output light intensity of the lamp is 120 V, 11A. For each test, 12 mg catalyst powder is added into 10 mL of 20 mg/L MB solution. Before light irradiation, the suspensions are firstly ultrasonically dispersed in dark for 2 min and then magnetically stirred in dark for 5 min to reach adsorption-desorption equilibrium. After photocatalytic degradation, the reaction suspension is centrifuged at 11,500 rpm for 5 min to remove the catalyst powder. Then, 5 mL supernatants are extracted and analyzed at 664 nm on the UV–vis spectrophotometer to evaluated corresponding MB degradation efficiencies.

3. Results and discussion

3.1. XRD analysis

Fig. 1 shows the XRD patterns of these adsorbents before adsorption. All adsorbents show the predominant characteristic peaks of $\text{Ca}_{1.5}\text{Si}_5\text{O}_{3.5} \cdot x\text{H}_2\text{O}$ (PDF card 33-0306) at 2θ of 29.36° and 32.05°, which indicates that these adsorbents are CSH-based adsorbents. As shown in Fig. 1a, the peaks locate at 15.73°, 25.32°, 26.92°, 30.04°, 32.86°, 35.7°, 40.04°, 42.17°, 50.05°, and 54.97° are the characteristic diffraction of tobermorite (PDF card 45-1480, $\text{Ca}_5\text{Si}_6(\text{O}, \text{OH}, \text{F})_{18} \cdot 5\text{H}_2\text{O}$), which means the predominant composition of CSH is tobermorite. After modification with F, the diffraction peaks are mainly observed at 2θ of 28.27°, 32.76°, 47.00°, 55.76°, 68.67° and 75.85°, which can be inferred that the main composition of F-CSH is fluorite (PDF card 35-0826, CaF_2 , Fig. 1b). During the process of modification, partial sites of silicate ions are

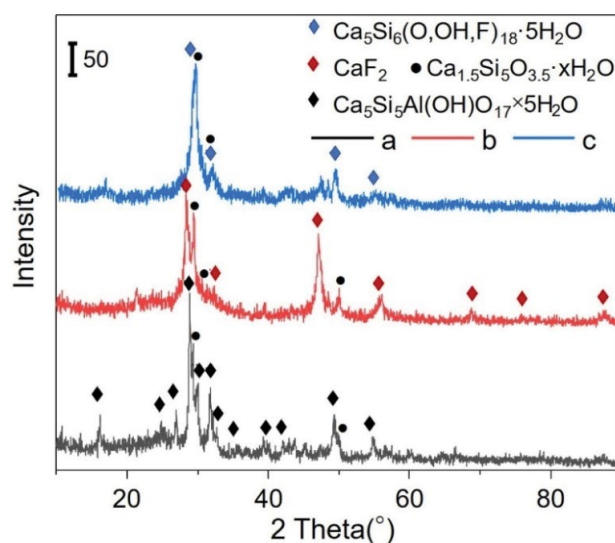


Fig. 1. XRD patterns of adsorbents before adsorption: (a) CSH, (b) F-CSH, and (c) Al-CSH.

occupied by fluoride ions in the hydrothermal reaction process and these fluoride ions react with Ca^{2+} to form the cubic packed CaF_2 . After modification with Al, the composition of adsorbent is mainly aluminum tobermorite and the diffraction peaks are mainly observed at 2θ of 29.81°, 31.77°, 49.27°, and 54.76° (PDF card 19-0052 $\text{Ca}_3\text{Si}_5\text{Al}(\text{OH})\text{O}_{17} \cdot 5\text{H}_2\text{O}$ Fig. 1c), and the partial characteristic peaks of $\text{Ca}_5\text{Si}_6(\text{O}, \text{OH}, \text{F})_{18} \cdot 5\text{H}_2\text{O}$ located at 2θ of 15.73°, 25.32°, and 26.92° disappear. This is probably due to the fact that Al reacted with OH to produce Al–OH amorphous complex group.

XRD patterns of these adsorbents after adsorption of Cr are shown in Fig. 2. Obviously, several new peaks are emerged by comparing the XRD patterns adsorbents before adsorption of Cr, which indicates the crystal structure of adsorbents has been changed after adsorption. The characteristic peaks locate at 2θ of 16.01°, 25.80°, 37.30° and 45.33° (Fig. 2a) indicate the formation of CaCr_2O_4 , which shows the interaction between chromium and calcium. From the XRD patterns of Al-CSH after adsorption, it can be clearly found that the characteristic peaks of $\text{Ca}_3\text{Si}_5\text{Al}(\text{OH})\text{O}_{17} \cdot 5\text{H}_2\text{O}$ Fig. 1c at 2θ of 49.27° and 54.76° disappear, while the characteristic peaks of Cr_2O_3 appear at 7.15° and 28.25°. This phenomenon indicates that the crystal morphology of Al-CSH changes after Cr adsorption.

3.2. N_2 adsorption–desorption analysis

Textural properties of adsorbents before and after Cr adsorption, including BET-surface area, pore-volume, and the pore diameter, is measured by N_2 adsorption–desorption technique and the results are listed in Table 1. For the adsorbents before adsorption, Al-CSH possesses the maximum specific surface area and pore volume which may be due to the exchange of Ca and Al in the calcium silicate during the modification, while the atomic radius of Al is slightly smaller than that of Ca, after the replacement of Ca by Al, there are more bonding voids in the material and thereby enhances the porosity in the structure of calcium

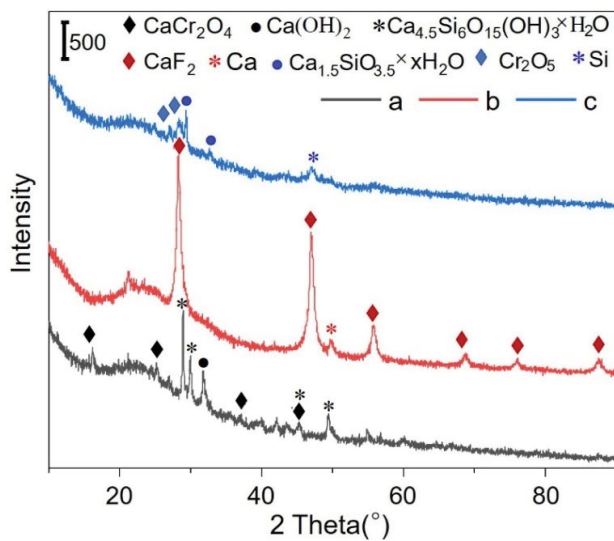


Fig. 2. XRD patterns of different adsorbents after adsorption: (a) CSH, (b) F-CSH, and (c) Al-CSH.

Table 1
Textural properties of adsorbents before and after Cr adsorption

Adsorbent		S_{BET} (m ² /g)	Pore volume (cm ³ /g)	Pore diameter (nm)
CSH	before	122.13	0.695	24.52
	after	207.91	0.766	20.29
Al-CSH	before	172.33	0.980	24.23
	after	208.71	0.691	18.40
F-CSH	before	94.77	0.511	20.76
	after	161.14	0.564	19.61

silicate adsorbent. These excellent features combined together contribute to Al-CSH the best performance for Cr adsorption. The chromium ions enter into the interlayer of CSH and occupy the original pore channels [23,24], which makes the original large pore segmentation generate more pores, thus reducing the pore diameter and increasing the specific surface area, which caused the specific surface area of all adsorbents increased and pore diameter decreased after Cr adsorption by comparing with the adsorbents before adsorption (Table 1).

3.3. Scanning electron microscopy

SEM images of the adsorbents before and after adsorption are shown in Fig. 3. It is obvious that all adsorbents before adsorption possess a rough surface [25] (Figs. 3a, c, and e), which is beneficial for capturing Cr ions. However, Al-CSH has more flourishing pores and better mesh structure compared with the CSH and F-CSH. The Al-CSH has the largest specific surface area and average pore volume, which confirms the results of Table 1. After adsorption, Cr ions enter into the pores of the adsorbent and thus the morphology of the adsorbents change significantly from a coral-like shape to a full coating (Figs. 3b, d, and f). It is

consistent with the morphology changes in XRD patterns (Figs. 1 and 2).

3.4. Adsorption kinetics

To explore the adsorption properties of these adsorbents and fully understand the dynamic interaction of Cr(III) with adsorbents, adsorption kinetic experiments are carried out at 25°C with an adsorbent dosage of 1.25 g/L. The extent of Cr(III) removal by the three adsorbents is found to increase with the increase in contact time. Chemisorption and the external surface adsorption can be used to explain the fast adsorption during the initial stage in Fig. 4. It is observed that a large number of vacant sites are available initially for the absorption of Cr(III) metal ion, so the adsorption of Cr(III) is fast. But with the passage of time, the remaining vacant sites are occupied by the Cr(III) [26]. As shown in Fig. 4, the adsorption equilibrium time of Al-CSH and CSH is 60 and 90 min respectively, while the F-CSH has a time of 150 min to reach the adsorption equilibrium. Thus, we can conclude that Al-CSH adsorbent exhibits the best adsorption capacity, which is contributed by its excellent textural properties.

3.5. Dynamic adsorption

Because of the extensive applicability of Eqs. (3) and (4) [27], these two equations are selected to study the dynamic adsorption of the three adsorbents for Cr.

Pseudo-first-order equation:

$$\ln(q_e - q_t) = \ln q_e - k_1 t \quad (3)$$

Pseudo-second-order equation:

$$\frac{t}{q_t} = \frac{1}{k_2 q_e^2} + \frac{t}{q_e} \quad (4)$$

where, q_e (mg/g) is the amount of equilibrate adsorption capacity, q_t (mg/g) is the amount of metal ion adsorption capacity at a certain time t (min). The k_1 (min⁻¹) and k_2 (g mg⁻¹ min⁻¹) are the constants of the pseudo-first-order and pseudo-second-order equations, respectively. The experimental values and simulation results of the pseudo-first-order model and pseudo-second-order model are shown in Figs. 5 and 6, and the kinetic parameters are shown in Table 2. It is apparent from Table 2 that the values of correlation coefficients (R^2) of the pseudo-first-order model are lower than the pseudo-second-order model which indicates that the pseudo-second-order model is better obeyed than pseudo-first-order model [28]. Consequently, the adsorption process appears to follow pseudo-second-order reaction kinetics, suggesting that the process is mainly controlled by chemisorption [29,30].

The adsorption process typically involves the diffusion of solute molecules into the pores to bind with the adsorption sites, and an intraparticle diffusion model is used to further describe the adsorption process in our work. The Fig. 7 indicates the Cr(III) adsorption process can be divided into three stages (shown in linear terms). The diffusion of

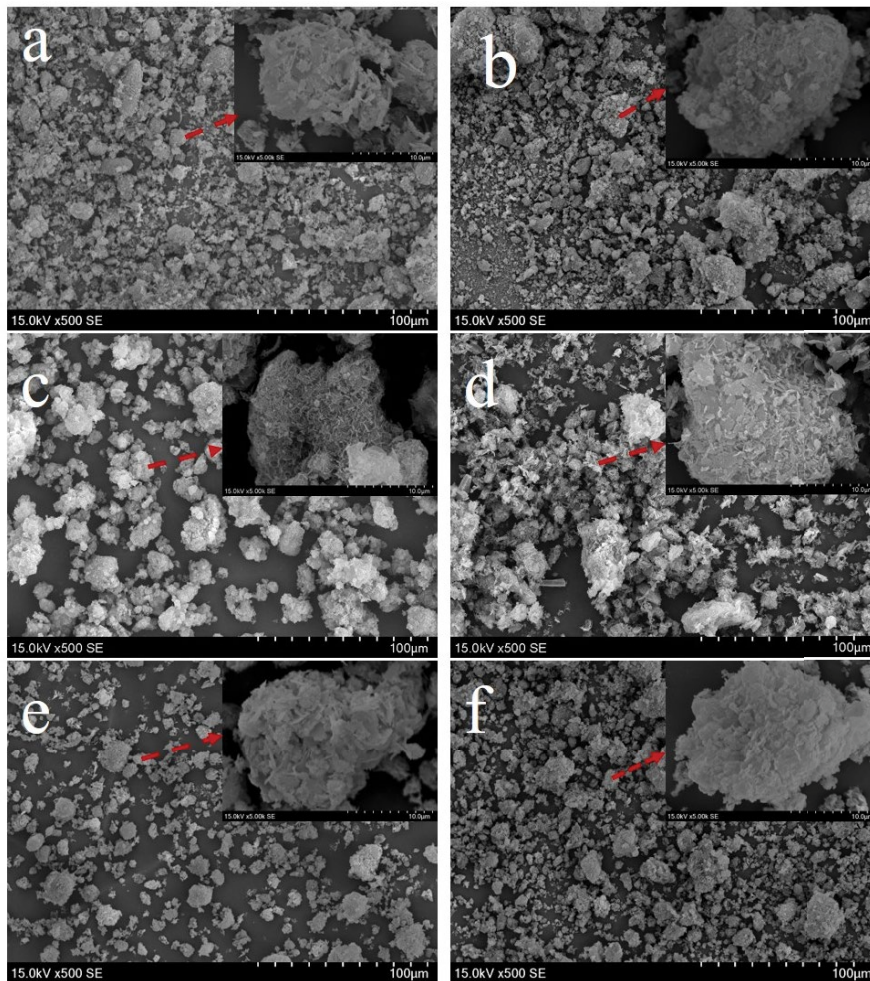


Fig. 3. (a and b) SEM images of three adsorbents before (a, c and e) and after (b, d, and f) adsorption, (c and d) unmodified adsorbent, (e) Al-CSH and (f) F-CSH.

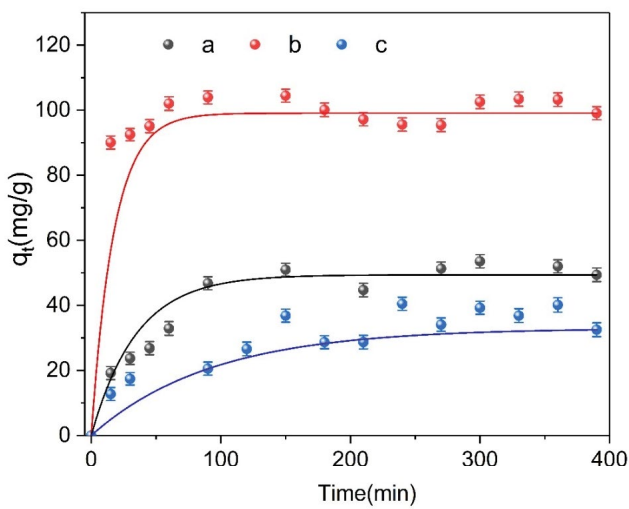


Fig. 4. Adsorption of Cr(III) ions by different adsorbents (solution pH = 3, adsorbent dosage = 1.25g/L, initial concentration of Cr(III) = 400 mg/L and temperature = 298 K). (a) CSH, (b) Al-CSH, and (c) F-CSH.

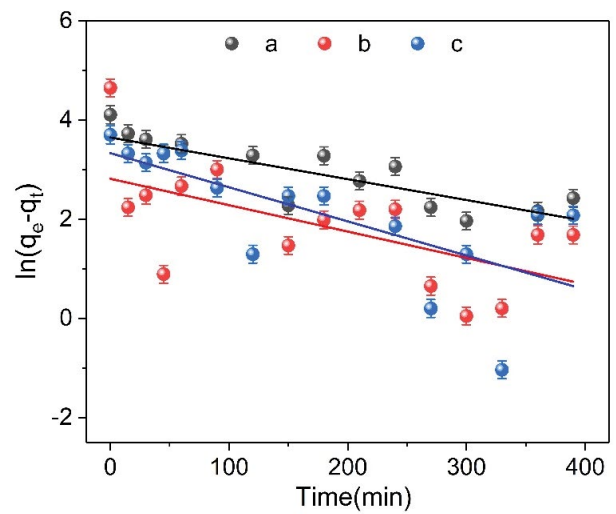


Fig. 5. Linearized pseudo-first-order kinetic plots for Cr(III) adsorption by different adsorbents. (a) CSH, (b) Al-CSH, and (c) F-CSH.

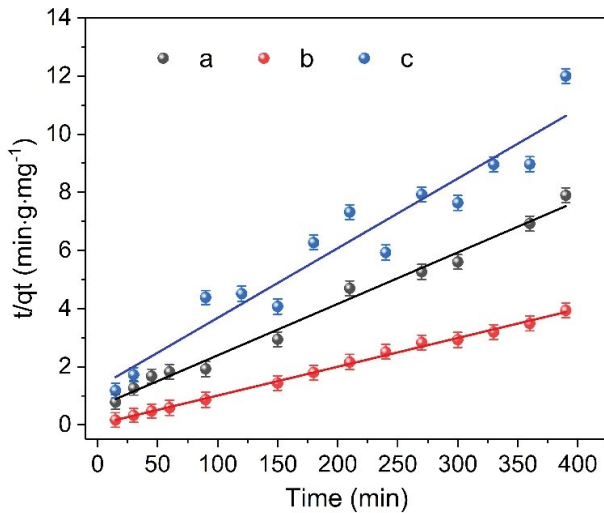


Fig. 6. Linearized pseudo-second-order kinetic plots for Cr(III) adsorption by different adsorbents. (a) CSH, (b) Al-CSH, and (c) F-CSH.

Cr(III) ions from the aqueous solution to the external surface of the adsorbent is represented by the first steep slope. The second slope is the diffusion of the Cr(III) ions into the pores of the adsorbent, which is the rate-determining step [31]. When the Cr(III) ions diffuse into the pores of the adsorbent, some chromium complexes are formed, and the objects narrow the pore channels, thus causing the rate of the second segment to decrease. The third slope is the equilibrium process in which Cr(III) ions are adsorbed on the adsorption sites in the inner surface of the pores, and intra-particle diffusion begins to slow down because of the decrease in chromium concentration in the bulk of the solution as the adsorption process proceed.

For physical adsorption, small pore size is favorable for capturing more ions. For chemisorption, a large surface area can provide more active sites for adsorption. Comparing the three adsorbents, the Al-CSH shows the largest BET surface area, relatively small pore diameter and a relatively large amount of Cr(III) adsorption, so the subsequent optimum conditions for removing Cr(III) are studied by using Al-CSH.

3.6. Effect of initial pH

Generally, the pH value will influence the adsorption performance [32]. Considering the hydrolysis of metal ions

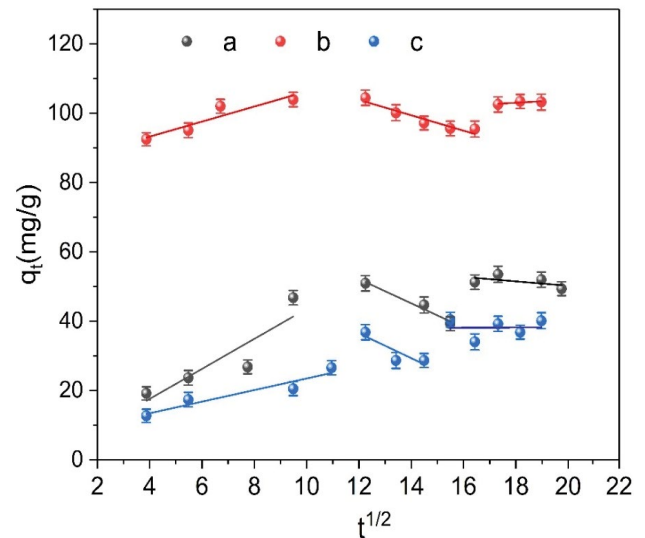
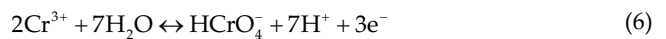
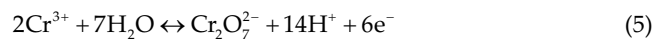


Fig. 7. Intra-particle diffusion model.

and the dissolution of the adsorbent, the pH of the wastewater ranges from 2.2 to 3.6 is selected in our experiments. From Fig. 8, it can be clearly observed that the amount of adsorption always increases by increasing the pH value from 2.2 to 3.6. The function of pH can be explained by Eqs. (5) and (6) with electrostatic attraction and redox mechanism [32,33].



The concentration of H^+ in the solution is reflected by pH value. This means that the pH value decreases with the increase of H^+ concentration. Consequently, the process Cr^{3+} transforms into $\text{Cr}_2\text{O}_7^{2-}$ or HCrO_4^- is accelerated by decreasing the concentration of H^+ . Thus, in this case, $\text{Cr}_2\text{O}_7^{2-}$ and HCrO_4^- are more easily to be adsorbed by changing the pH value [32,34]. On the other hand, the increase of adsorption capacity of Cr(III) with increasing pH is due to the fact that the concentration of negative charge on the surface of Al-CSH is increased which adsorbed the cationic ions more efficiently [35].

Table 2
Kinetic parameters for Cr(III) adsorption by different adsorbents

Adsorbent	q_e (mg/g) _{exp} ^a	Pseudo-first-order kinetics			Pseudo-second-order kinetics		
		q_e (mg/g) _{cal1} ^b	k_1 (min ⁻¹)	R_1^2	q_e (mg/g) _{cal2}	k_2 (min ⁻¹)	R_2^2
CSH	61.7	41.99	0.0051	0.6663	56.34	0.000516	0.9871
Al-CSH	104.5	11.03	0.0067	0.3691	101.01	0.005475	0.9965
F-CSH	40.5	35.93	0.0131	0.4667	41.70	0.000453	0.9282

^a q_e (mg/g)_{exp}, experimental values obtained from Fig. 4; ^b q_e (mg/g)_{cal}, theoretical values calculated by Eq. (4).

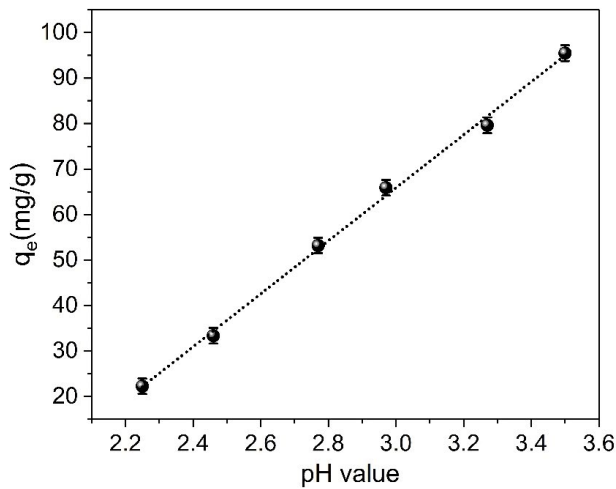


Fig. 8. Relationship between absolute adsorption capacity vs. pH value of wastewater. (Adsorption time: 60 min; adsorbent dosage: 1.5 g/L; initial concentration of Cr(III): 400 mg/L; temperature: 298 K).

3.7. Effect of adsorbent dose

Fig. 9 shows the effect of adsorbent dose on the Cr(III) removal efficiency and absolute adsorption capacity. It can be clearly observed that both the Cr(III) removal efficiency and absolute adsorption capacity increase by increasing adsorbent dose from 0 to 2.5 g/L. This is an expected result because more adsorption sites for Cr adsorption are offered by increasing the adsorbent dose. However, when the adsorbent dose further increases from 2.5 to 3 g/L, the Cr(III) removal efficiency keeps almost unchanged at 100% and the absolute adsorption amount decreases from 160 to 135 mg/g as shown in Fig. 9, which might be due to the aggregation of Al-CSH particles causing a decrease in adsorbent total surface area and increased the diffusional path [36].

3.8. Adsorption isotherms

Adsorption isotherm can be used to evaluate the adsorption capacities of adsorbents and to describe the interaction between adsorbates and adsorbents [25]. To better understand the mechanism of Cr(III) removal, four typical adsorption isotherm models, Langmuir Eq. (7), Freundlich Eq. (9), TemkinEq. (10), and DR Eq. (11) models are used to analyze the equilibrium data. Their linear Eq. (7) are expressed as follows [29,37]:

$$\text{Langmuir: } \frac{C_e}{q_e} = \frac{1}{K_L q_m} + \frac{C_e}{q_m} \quad (7)$$

where C_e (mg/L) is the equilibrium concentrations of Cr(III) in the liquid phase, q_e (mg/g) is the equilibrium concentrations of Cr(III) in the adsorbents, q_m (mg/g) is the maximum adsorption amount, and K_L (L/mg) is the Langmuir coefficient related to surface adsorption energy [37]. Meanwhile,

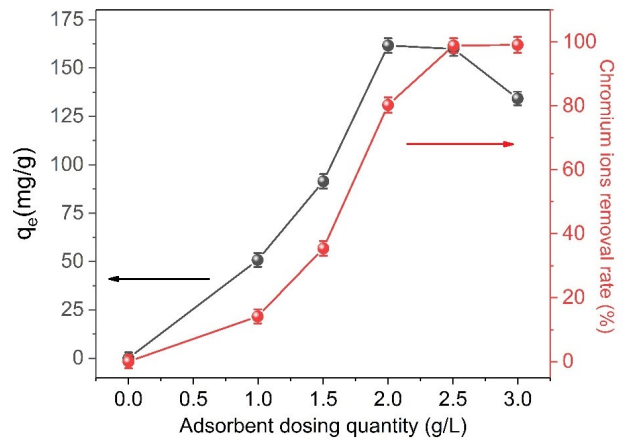


Fig. 9. Cr(III) removal efficiency and absolute adsorption amount vs. adsorbent dose. (Adsorption time = 60 min, solution pH = 3.18, initial concentration of Cr(III) = 400 mg/L and temperature = 298K).

a dimensionless constant (R_L) is expressed in Eq. (8), which is used to find out the applicability of the Langmuir model.

$$R_L = \frac{1}{1 + K_L C_0} \quad (8)$$

where, C_0 is the initial concentration of Cr(III), and K_L is Langmuir constant. Irreversible equilibrium when $R_L = 0$, favorable equilibrium when $0 < R_L < 1$, linear case when $R_L = 1$ or unfavorable equilibrium when $R_L > 1$ [25]. The value of R_L is greater than zero and less than unity which indicated the favorable adsorption of Cr(III) onto Al-CSH [28].

$$\text{Freundlich: } \ln q_e = \ln K_F + \frac{1}{n} \ln C_e \quad (9)$$

where K_F is the Freundlich parameter related to the adsorption amount, and n is the Freundlich parameter related to the intensity of adsorption, the larger the value of n , the better the adsorption performance. The value of $n > 1$ for Cr(III) indicated the favorable adsorption by Al-CSH at different concentrations [38].

$$\text{Temkin: } q_e = B \ln A + B \ln C_e \quad (10)$$

where A and B are Temkin constants, $B = RT/Z$, R is the gas constant with a value of 8.314 J/(mol K), T (K) is the absolute temperature, and Z (J/mol) is the Temkin isotherm adsorption heat.

$$\text{DR: } \ln q_e = \ln q_m - b \varepsilon^2 \quad (11)$$

where $\varepsilon = RT \ln(1 + C_e^{-1})$, ε is the Polanyi potential energy, b is the activity coefficient related to adsorption, moreover, the constant b gives the mean free energy E (kJ/mol), which is an important parameter to determine the adsorption mechanism, and can be computed using Eq. (12). It is generally

considered that $E < 8$ kJ/mol represents physical adsorption, and the adsorption mechanism can be explained by ion-exchange when E varies from 8 to 16 kJ/mol.

$$E = 2b^{-0.5} \quad (12)$$

The parameters obtained from the linearization are shown in Table 3, Cr(III) adsorption equilibrium isotherms onto the Al-CSH are depicted in Fig. 10. As listed in Table 3, The R_L value calculated is 2.46×10^{-4} , suggests the adsorption process is favorable at operating conditions. The adsorption of Cr(III) by Al-CSH agreed with the Langmuir model best, suggesting that the adsorption process is proceeded through monolayer adsorption [25]. Moreover, this result can also be demonstrated by the $1/n$ value from Table 3. The energy E value calculated by the DR model is 14.37 kJ/mol, which shows the adsorption process follows the ion-exchange mechanism.

3.9. Thermodynamic studies

Investigating the thermodynamics of Cr(III) adsorption will allow for a better understanding of the driving force behind the adsorption characteristics, adsorption process and mechanisms. As shown in Fig. 11, the adsorptive capacity of the adsorbents decreases with the increases in reaction temperature. Thermodynamic parameters are calculated by the Eq. (13).

$$\ln K_d = \frac{\Delta S^\circ}{R} - \frac{\Delta H^\circ}{RT} \quad (13)$$

where ΔH° , ΔS° , and T are the enthalpy, entropy, and temperature in Kelvin, respectively. K_d is the partition coefficient of adsorption, and its value is calculated according to $K_d = q_e/C_e$ [32]. The values of ΔH° , ΔS° are obtained from the slope and intercept of $\ln K_d$ vs. $1/T$ ($R^2 = 0.9403$, Fig. 12), R is the gas constant.

Table 3
Best fit parameters obtained from fitting the adsorption of Cr(III) to Al-CSH

Model	Linear form	Parameters obtained from linearization	
Langmuir	$\frac{C_e}{q_e} = \frac{1}{K_L q_m} + \frac{C_e}{q_m}$	R^2	0.9992
		q_m (mg/g)	160.26
		K_L (L/mg)	13.56
		R_L	2.46×10^{-4}
Freundlich	$\ln q_e = \ln K_F + \frac{1}{n} \ln C_e$	R^2	0.9926
		K_F (mg/g)	152.82
		n^{-1}	0.16389
Temkin	$q_e = B \ln A + B \ln C_e$	R^2	0.9869
		Z (J/mol)	115.63
DR	$\ln q_e = \ln q_m - b \varepsilon^2$	R^2	0.9919
		q_m (mg/g)	158.09
		E (kJ/mol)	14.37

The Gibbs free energy of specific adsorption is calculated from the well-known Eq. (14):

$$\Delta G^\circ = \Delta H^\circ - T\Delta S^\circ \quad (14)$$

The thermodynamic parameters for the adsorption of Cr(III) ions on adsorbent are given in Table 4, which shows that the adsorption isotherm at 286 K which is higher than the other isotherms. Whereas, the adsorption isotherm at $T = 310$ K is the lowest. The results indicate that the adsorption of Cr(III) on Al-CSH is favored at low temperatures. The negative value of enthalpy change, ΔH° , indicates that the adsorption of Cr(III) is an exothermic process [39]. The positive value of ΔS° designates the affinity of Al-CSH for Cr(III) and the increases disorder at the solid/liquid interface during the adsorption process [28] and also attributes to enhancement in the degree of freedom during the adsorption of Cr(III) metal ion from aqueous solution [26,35]. Adsorption of cations (in this case, may indicate that the number of ions displaces from the solid surface is greater than the number of adsorbed ions, which means that three divalent Ca ions can be exchanged for two Cr(III) ions [40]). The negative values of ΔG° indicate that Cr(III) sorption is spontaneous in all cases.

3.10. Possible mechanism about adsorption

According to the Langmuir isotherm, we have indicated the adsorption process of Al-CSH for Cr belongs to monolayer adsorption. From the EDS results (Figs. 13d and e), it can be clearly observed the content of Cr on the surface of the Al-CSH significantly increases from 0% (wt.%) to 11.63% (wt.%), while the content of Ca decreases from 22.94% (wt.%) to 1.91% (wt.%) after adsorption. This suggests the adsorption process of Al-CSH for Cr proceeds through an ion-exchange mechanism, during which Ca is replaced by Cr. From the XPS results shown in Fig. 13, the peak intensity of calcium at 374.2 and 350.7 eV decreases and obvious chromium peaks at 576.6, 577.6, 586.9 and 598.56 eV appear, which indicates that the calcium is replaced by chromium on the surface of adsorbent after adsorption. The chromium adsorbed on the surface of the adsorbent is mainly present in the form of Cr_2O_3 ($2P_{3/2}$, 576.63 eV [41], $2P_{3/2}$, 587.1 eV [42]), CrO_x ($2P_{3/2}$, 576.6 eV [43]), $\text{Cr}(\text{OH})_3$ ($2P_{3/2}$, 577.4 eV [44], $2P_{1/2}$, 586.8 eV [45]), $\text{Cr}(\text{NO}_3)_3$ ($2P_{3/2}$, 577.3 eV [46], $2P_{1/2}$, 587 eV [45]). From the XPS spectra shown in Fig. 13, the binding energy of O shifts to a lower energy level, while the binding energy of Si shifts to a higher energy level, indicating the formation of the interaction between Cr, Si and O. Based on the above results, the adsorption mechanism of Cr(III) ions by ion exchange in monolayer can be obtained in this work (Fig. 14). The Al-CSH works as the crystal seed [47] to promote the replacement of Cr for Ca on the adsorbent, and further crystallize the deformable apatite crystals in our tested pH range with the existence of silicate.

3.11. Process verification

To further verify the efficiency of Al-CSH, the test is carried out in a waste solution which contains 410 mg/L chromium (III) with an initial pH of 3.18 under the room

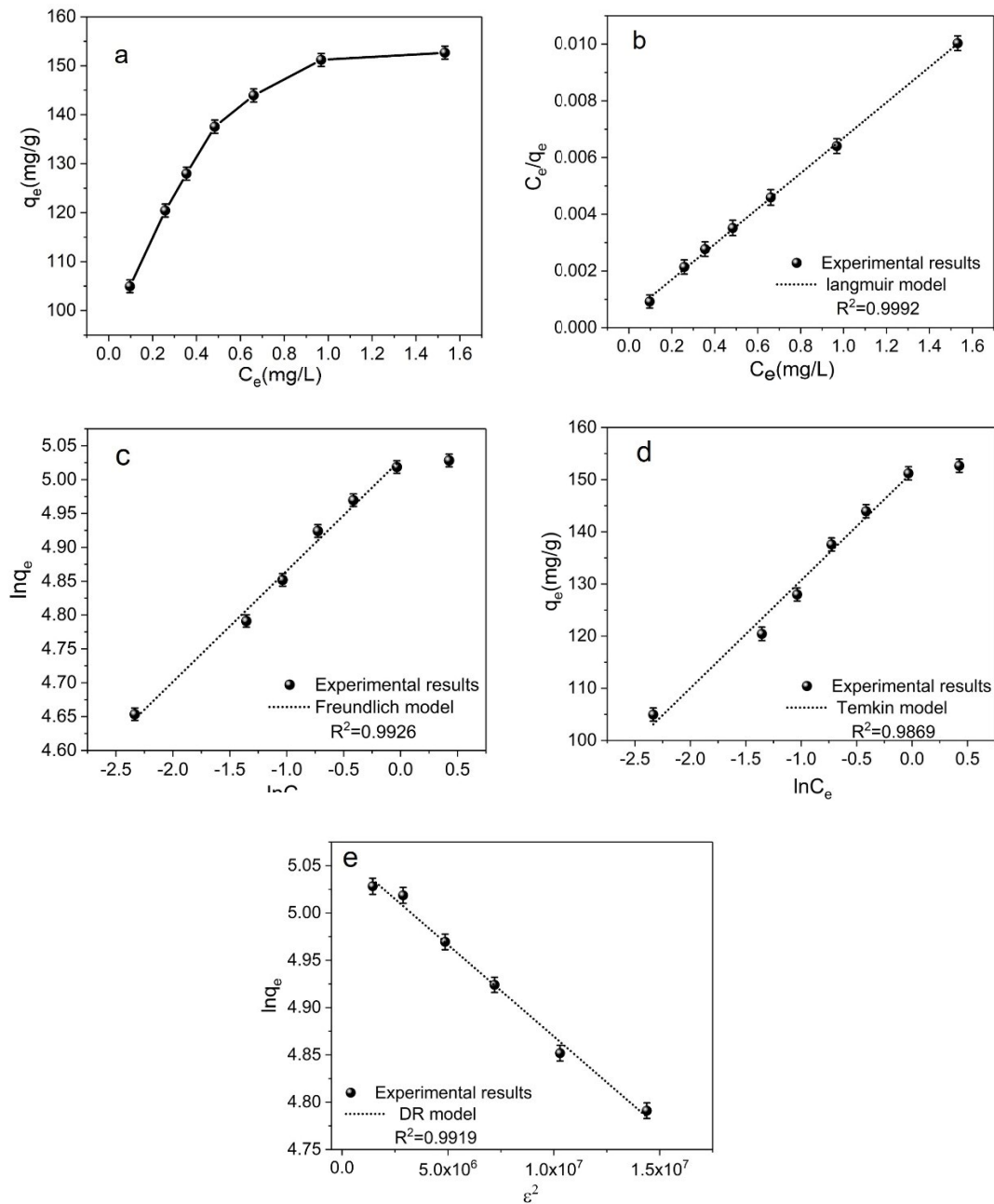


Fig. 10. Adsorption isotherm of Cr(III) ions onto Al-CSH. (a) Adsorption isotherm (adsorption time = 120 min, solution pH = 3.18, adsorbent dosage = 2 g/L and temperature = 288 K), (b) Langmuir model, (c) Freundlich model, (d) Temkin model, and (e) R model.

temperature. To our delight, the concentration of Cr(III) in the wastewater is reduced to 0.97 mg/L after adsorption, which meets the discharge standard in China (GB 8978-1996, 1.5 mg/L). Furthermore, Al-CSH is applied to the treatment of multi-metal mixed wastewater (mainly containing Cr, Cu and Ni). The concentration of Cr, Cu and Ni in wastewater decreased from 140.2, 150.6, 145.1 to 0.08, 0.08, and 0.07 mg/L respectively, which shows the universal ability of Al-CSH for the removal of heavy metal ions in sewage. The removal efficiency of Al-CSH to Cr^{3+} , Cu^{2+} and Ni^{2+} is Cr^{3+} 99.943% < Cu^{2+} 99.947% < Ni^{2+} 99.951%, respectively. This is

due to the adsorption process of Al-CSH is an ion exchange process, the calcium ions in the adsorbent exchange with the heavy metal ions in the water, so the divalent metal ion is more easily exchanged, and the activity of Ni^{2+} is stronger than that of Cu^{2+} , so the removal rate of Ni^{2+} is the highest. Meanwhile, a general comparison of various well-studied adsorbents is listed in Table 5. Obviously, the Al-CSH can exceed or at least be comparable to most of the present hot adsorbents in terms of adsorption capacity and equilibrium time, which endows it with a strong potential industry application perspective.

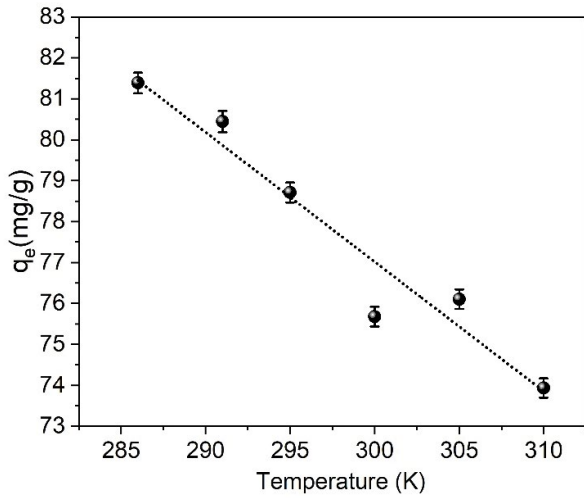


Fig. 11. Absolute adsorption capacity vs. reaction temperature. (Adsorption time = 60 min, solution pH = 3.18, initial concentration of Cr(III) = 400 mg/L and adsorbent dosage = 1.5 g/L).

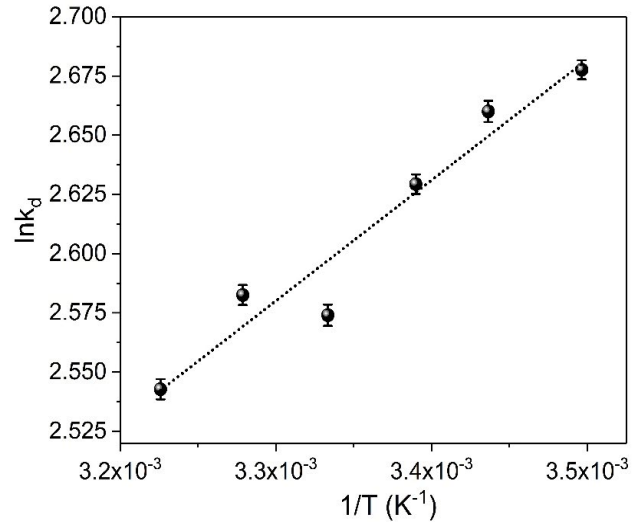


Fig. 12. Effect of temperature on the distribution coefficients of Cr(III) on Al-CSH.

Table.4
Mean values of thermodynamic parameters of Cr(III) adsorption

ΔH°	ΔS°	ΔG° (kJ/mol)					
kJ/mol	J/(mol K)	286 K	291 K	295 K	300 K	305 K	310 K
-4.24	7.47	-6.37	-6.41	-6.44	-6.47	-6.52	-6.55

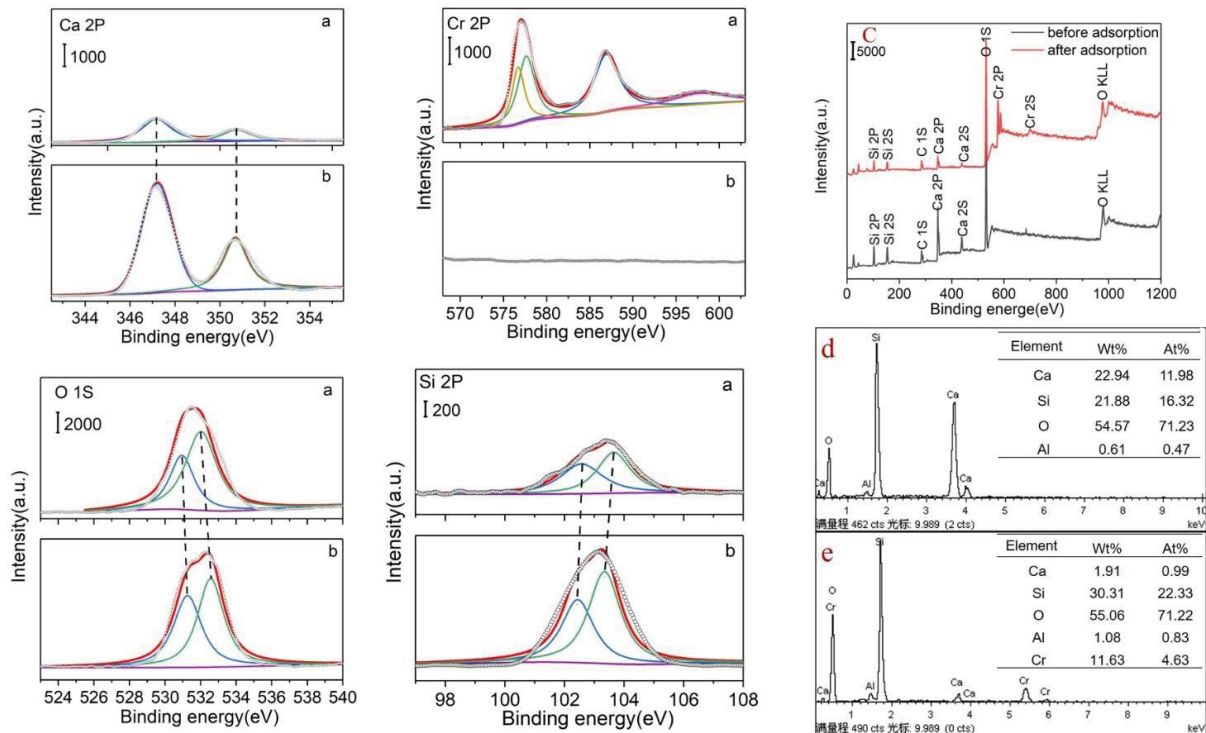


Fig. 13. XPS spectra of O 1s, Ca 2P, O 2P and Si 2P for Al-CSH before and after Cr adsorption, (a) after adsorption, (b) before adsorption, (c) XPS survey of Al-CSH before and after adsorption; EDS results of Al-CSH before and after adsorption, (d) before adsorption, and (e) after adsorption.

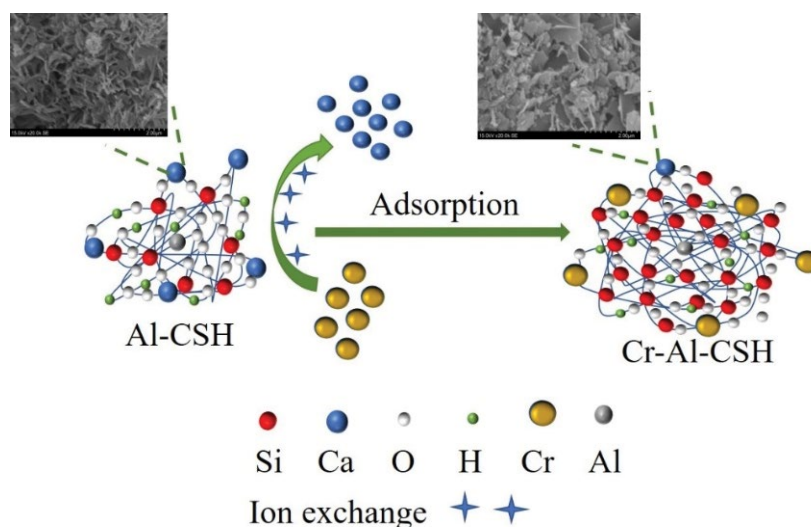


Fig. 14. Schematic diagram of adsorption mechanism.

Table 5

Comparison of variously reported adsorbents with Al-CSH for Cr(III) adsorption at ambient temperature (10°C–30°C)

Adsorbent type	Adsorption capacity (mg/g)	Equilibrium time (min)	Ref.
Apricot shells activated carbons	143.63	300–480	[48]
Wood activated carbons	158.03	300–480	[48]
Walnut shells activated carbons	105.22	300–480	[48]
Complex copper sulfide	52.3	120	[49]
Porous hydroxyapatite	96.9	NA	[50]
SDGPMA–SP–COOH	36.63	240	[51]
Al-CSH	160	60	This work

3.12. Reuse of the chromium-saturated Al-CSH composites as a photocatalyst

As the CSH hydrate adsorbs heavy metal ions through the release of OH^- and Ca^{2+} , it is difficult to recycle the CSH hydrate composites to re-adsorption of heavy metal ions [18]. In recent years, many researchers have doped the photocatalyst with heavy metal ions to increase the band gap [52]. The chromium enrichment, increase of micro-pore area and specific surface area of Al-CSH after adsorption lays a foundation for its reuse. Based on these, a method by which the Al-CSH bearing Cr(III) ions can be converted as a photocatalyst via a simple calcination process for the removal of organic dyes (e.g., methylene blue, MB) is presented in this work. After the Al-CSH loaded with Cr is heated at 300°C/air (Al-CSH-Cr), its photocatalytic activity is noted to be significantly improved, which is believed to be the result of the surface-coated Cr phase. The degradation efficiency of Al-CSH-Cr toward MB is approximately 94% after irradiation for 100 min. Moreover, the recycle photodegradation experiments are performed (Fig. 15), showing a very small change compared to the first cycle. In addition, to better evaluate the photocatalytic performance of the catalyst in this work, a comparison to recently reported photocatalysts for MB degradation is listed in Table 6. Overall,

the MB photodegradation performance of the Al-CSH-Cr is comparable to many well-studied catalysts and is superior to similar catalysts with CSH hydrate as the support (CSH-Cu). Our results demonstrate excellent reusability of the Al-CSH after the adsorption of Cr(III) as the photocatalyst.

4. Conclusions

In summary, fluorosilicic acid, a by-product of the wet-process of phosphoric acid is successfully applied to synthesize the Al-CSH adsorbent for Cr removal. The adsorption capacity of Al-CSH can reach to 160 mg/g. The adsorption of Cr(III) fits with the Langmuir isotherm best and follows the pseudo-second-order kinetic model. Moreover, the adsorption process proceeded through a cation exchange adsorption mechanism. Additionally, the adsorbent has shown an excellent universality for the removal of heavy metal ions, including Ni, Cu and Cr. Most importantly, the Al-CSH adsorbent containing Cr(III) ions after adsorption could be converted into an efficient photocatalyst for MB degradation, and the degradation efficiency could up to 94% under the simulated sunlight within 100 min. The route of the “waste → adsorbent → catalyst” proposed in this work illuminates a promising direction for

Table 6
Comparison of photocatalytic performance of various photocatalysts for degradation of MB

Photocatalyst	Catalyst dose (g/L) and MB conc. (mg/L)	Degradation efficiency (%) vs. contact time (min)	Ref.
g-C ₃ N ₄	2.5 of 10	~99 vs. 75	[53]
CSH-TiO ₂	0.5 of ~75	96.2 vs. 300	[54]
CSH-CuO	0.4 of 20	90 vs. 150	[18]
Mpg-C ₃ N ₄ /SnCoS ₄	0.2 of 20	95 vs. 160	[55]
Cu/Cu ₂ O NWs	4.67 of 20	90.6 vs. 120	[56]
Al-CSH-Cr	1.2 of 20	~94 vs. 100	This work

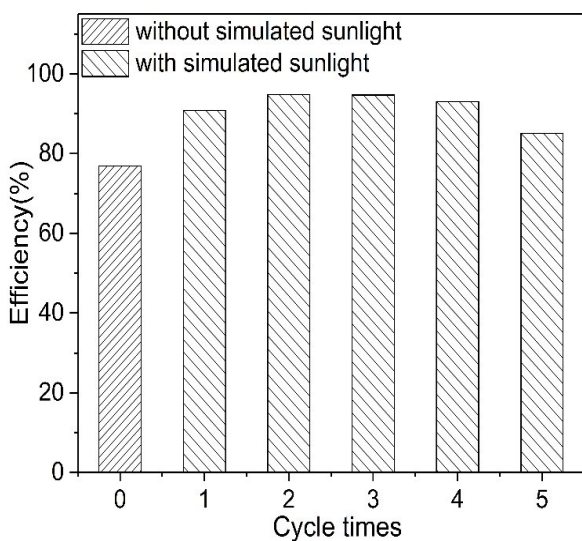


Fig. 15. MB removal efficiencies by Al-CSH-Cr vs. reused cycles.

waste utilization and water purification, which shows great significance for industrial application.

Acknowledgements

The authors gratefully acknowledge financial support from the Chinese National Natural Science Foundation (21776181), Sichuan University innovation spark project (2018SCUH0012), Chinese National Key Research and Development Plan (2018YFC1900203-03) and Central Universities in China (2030704401004).

References

- [1] A.K. Golder, A.K. Chanda, A.N. Samanta, S. Ray, Removal of hexavalent chromium by electrochemical reduction-precipitation: an investigation of process performance and reaction stoichiometry, *Sep. Purif. Technol.*, 76 (2011) 345–350.
- [2] J. Luo, J. Li, Y. Qi, Y. Cao, Study on the removal of chromium(III) by solvent extraction, *Desal. Water Treat.*, 51 (2013) 2130–2134.
- [3] T. O'Brien, Complexities of chromium carcinogenesis: role of cellular response, repair and recovery mechanisms, *Mutat. Res. Fundam. Mol. Mech. Mutagen.*, 533 (2003) 3–36.
- [4] X. Li, Y. Li, Z. Ye, Preparation of macroporous bead adsorbents based on poly(vinyl alcohol)/chitosan and their adsorption properties for heavy metals from aqueous solution, *Chem. Eng. J.*, 178 (2011) 60–68.
- [5] S. Arris, M. Bencheikh Lehocine, A.-H. Meniai, Sorption study of chromium sorption from wastewater using cereal by-products, *Int. J. Hydrogen Energy*, 41 (2016) 10299–10310.
- [6] A. Bhattacharya, T. Naiya, S. Mandal, S. Das, Adsorption, kinetics and equilibrium studies on removal of Cr(VI) from aqueous solutions using different low-cost adsorbents, *Chem. Eng. J.*, 137 (2008) 529–541.
- [7] O. Kusku, B.L. Rivas, B.F. Urbano, M. Arda, N. Kabay, M. Bryjak, A comparative study of removal of Cr(VI) by ion exchange resins bearing quaternary ammonium groups, *J. Chem. Technol. Biotechnol.*, 89 (2014) 851–857.
- [8] V.K. Gupta, I. Ali, T.A. Saleh, A. Nayak, S. Agarwal, Chemical treatment technologies for waste-water recycling—an overview, *RSC Adv.*, 2 (2012) 6380–6388.
- [9] B. Rezaei, O. Rahmanian, Direct nanolayer preparation of molecularly imprinted polymers immobilized on multiwalled carbon nanotubes as a surface-recognition site and their characterization, *J. Appl. Polym. Sci.*, 125 (2012) 798–803.
- [10] K. Okano, M. Uemoto, J. Kagami, K. Miura, T. Aketo, M. Toda, K. Honda, H. Ohtake, Novel technique for phosphorus recovery from aqueous solutions using amorphous calcium silicate hydrates (A-CSHs), *Water Res.*, 47 (2013) 2251–2259.
- [11] N. Shao, S. Li, F. Yan, Y. Su, F. Liu, Z. Zhang, An all-in-one strategy for the adsorption of heavy metal ions and photodegradation of organic pollutants using steel slag-derived calcium silicate hydrate, *J. Hazard. Mater.*, 382 (2020) 121120.
- [12] A. Baldermann, A. Landler, F. Mittermayr, I. Letofsky-Papst, F. Steindl, I. Galan, M. Dietzel, Removal of heavy metals (Co, Cr, and Zn) during calcium–aluminum–silicate–hydrate and trioctahedral smectite formation, *J. Mater. Sci.*, 54 (2019) 9331–9351.
- [13] Z. Zhang, X. Wang, H. Wang, J. Zhao, Removal of Pb(II) from aqueous solution using hydroxyapatite/calcium silicate hydrate (HAP/C-S-H) composite adsorbent prepared by a phosphate recovery process, *Chem. Eng. J.*, 344 (2018) 53–61.
- [14] L. Lihua, T. Li, G. Yang, Y. Wang, A. Tang, Y. Ling, Synthesis of thiol-functionalized mesoporous calcium silicate and its adsorption characteristics for heavy metal ions, *J. Environ. Chem. Eng.*, 5 (2017) 6201–6215.
- [15] Z. Zhang, X. Wang, J. Zhao, Phosphate recovery from wastewater using calcium silicate hydrate (C-S-H): sonochemical synthesis and properties, *Environ. Sci. Water Res. Technol.*, 5 (2019) 131–139.
- [16] X. Wang, K. Zhao, B. Yang, T. Chen, D. Li, H. Wu, J. Wei, X. Wu, Adsorption of dibutyl phthalate in aqueous solution by mesoporous calcium silicate grafted non-woven polypropylene, *Chem. Eng. J.*, 306 (2016) 452–459.
- [17] J. Wu, Y.-J. Zhu, F. Chen, Ultrathin calcium silicate hydrate nanosheets with large specific surface areas: synthesis, crystallization, layered self-assembly and applications as excellent adsorbents for drug, protein, and metal ions, *Small*, 9 (2013) 2911–2925.
- [18] N. Shao, S. Tang, Z. Liu, L. Li, F. Yan, F. Liu, S. Li, Z. Zhang, Hierarchically structured calcium silicate hydrate-based nanocomposites derived from steel slag for highly efficient heavy metal removal from wastewater, *ACS Sustainable Chem. Eng.*, 6 (2018) 14926–14935.

- [19] Z. Zhang, Y. Wang, H. Zheng, D. Ming, Y. Zhang, X. Zi, J. Huang, Co-production of cryolite and sodium silicate from fluorosilicic acid, *Phos. Comp. Fert.*, 31 (2016) 37–40.
- [20] Y. Wang, Production of phosphatic compound fertilizer industry in 2016 and its developing trend in 2017 in China, *Phos. Comp. Fert.*, 32 (2017) 1–6.
- [21] X. Zhu, Z. Zhang, J. Shen, Kinetics and mechanism of adsorption of phosphate on fluorine-containing calcium silicate, *J. Wuhan Univ. Technol.*, 31 (2016) 321–327.
- [22] X. Zhu, J. Li, Y. Jin, Y. Guo, Preparation of porous hybrid adsorbents based on fluor(calcium silicate)/activated carbon and its application in the removal of iron (III) from ammonium phosphate solutions, *Arabian J. Chem.*, 13 (2020) 1551–1562.
- [23] B. Guo, B. Liu, J. Yang, S. Zhang, The mechanisms of heavy metal immobilization by cementitious material treatments and thermal treatments: a review, *J. Environ. Manage.*, 193 (2017) 410–422.
- [24] Z.A. Al-Othman, R. Ali, M. Naushad, Hexavalent chromium removal from aqueous medium by activated carbon prepared from peanut shell: adsorption kinetics, equilibrium, and thermodynamic studies, *Chem. Eng. J.*, 184 (2012) 238–247.
- [25] Y. Liu, W. Zhang, C. Zhao, H. Wang, J. Chen, L. Yang, J. Feng, W. Yan, Study on the synthesis of poly(pyrrrole methanes) with the hydroxyl in different substituent position and their selective adsorption for Pb^{2+} , *Chem. Eng. J.*, 361 (2019) 528–537.
- [26] G. Sharma, M. Naushad, A.H. Al-Muhtaseb, A. Kumar, M.R. Khan, S. Kalia, Shweta, M. Bala, A. Sharma, Fabrication and characterization of chitosan-crosslinked-poly(alginic acid) nanohydrogel for adsorptive removal of Cr(VI) metal ion from aqueous medium, *Int. J. Biol. Macromol.*, 95 (2017) 484–493.
- [27] B.K. Biswas, K. Inoue, K.N. Ghimire, S. Ohta, H. Harada, K. Ohto, H. Kawakita, The adsorption of phosphate from an aquatic environment using metal-loaded orange waste, *J. Colloid Interface Sci.*, 312 (2007) 214–223.
- [28] M. Naushad, Surfactant assisted nano-composite cation exchanger: development, characterization and applications for the removal of toxic Pb^{2+} from aqueous medium, *Chem. Eng. J.*, 235 (2014) 100–108.
- [29] A.O. Babatunde, Y.Q. Zhao, Equilibrium and kinetic analysis of phosphorus adsorption from aqueous solution using waste alum sludge, *J. Hazard. Mater.*, 184 (2010) 746–752.
- [30] I. Uzun, F. Guzel, Rate studies on the adsorption of some dyestuffs and p-nitrophenol by chitosan and monocarboxymethylated(mcm)-chitosan from aqueous solution, *J. Hazard. Mater.*, 118 (2005) 141–154.
- [31] X. Yang, T. Zhou, B. Ren, A. Hursthouse, Y. Zhang, Removal of Mn(II) by sodium alginate/graphene oxide composite double-network hydrogel beads from aqueous solutions, *Sci. Rep.*, 8 (2018) 10717.
- [32] Z. Wang, C. Ye, X. Wang, J. Li, Adsorption and desorption characteristics of imidazole-modified silica for chromium(VI), *Appl. Surf. Sci.*, 287 (2013) 232–241.
- [33] N.A. Awang, W.N. Wan Salleh, A.F. Ismail, N. Yusof, F. Aziz, J. Jaafar, Adsorption behavior of chromium(VI) onto regenerated cellulose membrane, *Ind. Eng. Chem. Res.*, 58 (2018) 720–728.
- [34] H. Su, Y. Chong, J. Wang, D. Long, W. Qiao, L. Ling, Nanocrystalline celluloses-assisted preparation of hierarchical carbon monoliths for hexavalent chromium removal, *J. Colloid Interface Sci.*, 510 (2018) 77–85.
- [35] A.A. Alqadami, M. Naushad, Z.A. Al-Othman, T. Ahmad, Adsorptive performance of MOF nanocomposite for methylene blue and malachite green dyes: kinetics, isotherm, and mechanism, *J. Environ. Manage.*, 223 (2018) 29–36.
- [36] E. Daneshvar, A. Vazirzadeh, A. Niazi, M. Kousha, M. Naushad, A. Bhatnagar, Desorption of methylene blue dye from brown macroalgae: effects of operating parameters, isotherm study, and kinetic modeling, *J. Cleaner Prod.*, 152 (2017) 443–453.
- [37] X. Zhu, J. Li, J. Luo, Y. Jin, D. Zheng, Removal of cadmium(II) from aqueous solution by a new adsorbent of fluor-hydroxyapatite composites, *J. Taiwan Inst. Chem. Eng.*, 70 (2017) 200–208.
- [38] T. Tatarchuk, N. Paliychuk, R.B. Bitra, A. Shyichuk, M. Naushad, I. Mironyuk, D. Ziolkovska, Adsorptive removal of toxic methylene blue and acid orange 7 dyes from aqueous medium using cobalt-zinc ferrite nanoadsorbents, *Desal. Water Treat.*, 150 (2019) 374–385.
- [39] D. Xu, Adsorption of Pb(II) from aqueous solution to MX-80 bentonite: effect of pH, ionic strength, foreign ions and temperature, *Appl. Clay Sci.*, 41 (2008) 37–46.
- [40] T. Shahwan, H.N. Erten, Temperature effects in barium sorption on natural kaolinite and chlorite-illite clays, *J. Radioanal. Nucl. Chem.*, 260 (2004) 43–48.
- [41] T.P. Moffat, R.M. Latanision, An electrochemical and X-ray photoelectron-spectroscopy study of the passive state of chromium, *J. Electrochem. Soc.*, 139 (1992) 1869–1879.
- [42] E. Kemnitz, A. Kohne, I. Grohmann, A. Lippitz, W.E.S. Unger, X-ray photoelectron and X-ray excited auger electron spectroscopic analysis of surface modifications of chromia during heterogeneous catalyzed chlorine fluorine exchange, *J. Catal.*, 159 (1996) 270–279.
- [43] P. Dolle, M. Alnot, J.J. Ehrhardt, A. Cassuto, Study by spectroscopy of photo-electrons of initial-stages of oxidation in polycrystalline chromium, *J. Electron. Spectrosc. Relat. Phenom.*, 17 (1979) 299–321.
- [44] D. Shuttleworth, Preparation of metal-polymer dispersions by plasma techniques-an eaca investigation, *J. Chem. Phys.*, 84 (1980) 1629–1634.
- [45] E. Desimoni, C. Malitesta, P.G. Zamboni, J.C. Riviere, An X-ray photoelectron spectroscopic study of some chromium oxygen system, *Surf. Interface Anal.*, 13 (1988) 173–179.
- [46] J.J. Wei, Q.J. Xue, Effects of synthetic additives on the friction and wear properties of a Cr_2O_3 coating, *Wear*, 176 (1994) 213–216.
- [47] S.A. Khan, Riazurrehman, M.A. Khan, Adsorption of chromium(III), chromium(VI) and silver(I) on bentonite, *Waste Manage.*, 15 (1995) 271–282.
- [48] X. Wei, Z. Wu, Z. Wu, B.-C. Ye, Adsorption behaviors of atrazine and Cr(III) onto different activated carbons in single and co-solute systems, *Powder Technol.*, 329 (2018) 207–216.
- [49] T. Ai, X. Jiang, Q. Liu, Chromium removal from industrial wastewater using *Phyllostachys pubescens* biomass loaded Cu-S nanospheres, *Open Chem.*, 16 (2018) 842–852.
- [50] Y. Si, J. Huo, Y. Hengbo, A. Wang, Adsorption kinetics, isotherms, and thermodynamics of Cr(III), Pb(II), and Cu(II) on porous hydroxyapatite nanoparticles, *J. Nanosci. Nanotechnol.*, 18 (2018) 3484–3491.
- [51] T.S. Anirudhan, P.G. Radhakrishnan, Chromium(III) removal from water and wastewater using a carboxylate-functionalized cation exchanger prepared from a lignocellulosic residue, *J. Colloid Interface Sci.*, 316 (2007) 268–276.
- [52] L. Gnanasekaran, R. Hemamalini, M. Naushad, Efficient photocatalytic degradation of toxic dyes using nanostructured TiO_2 /polyaniline nanocomposite, *Desal. Water Treat.*, 108 (2018) 322–328.
- [53] M. Tahir, C. Cao, F.K. Butt, F. Idrees, N. Mahmood, Z. Ali, I. Aslam, M. Tanveer, M. Rizwan, T. Mahmood, Tubular graphitic- C_3N_4 : a prospective material for energy storage and green photocatalysis, *J. Mater. Chem. A*, 1 (2013) 13949–13955.
- [54] J. Shi, Y. Kuwahara, T. An, H. Yamashita, The fabrication of TiO_2 supported on slag-made calcium silicate as low-cost photocatalyst with high adsorption ability for the degradation of dye pollutants in water, *Catal. Today*, 281 (2017) 21–28.
- [55] Q. Liang, J. Jin, M. Zhang, C. Liu, S. Xu, C. Yao, Z. Li, Construction of mesoporous carbon nitride/binary metal sulfide heterojunction photocatalysts for enhanced degradation of pollution under visible light, *Appl. Catal., B*, 218 (2017) 545–554.
- [56] W. Chen, Z. Fan, Z. Lai, Synthesis of core-shell heterostructured Cu/Cu₂O nanowires monitored by in situ XRD as efficient visible-light photocatalysts, *J. Mater. Chem. A*, 1 (2013) 13862–13868.